Supplementary Information

Potassium-rich antiperovskites K$_3$HTe and K$_3$FTe and their structural relation to lithium- and sodium-rich counterparts

Koji Okada,[a] Susumu Fujii,[b,c] Cédric Tassel,[a] Shenghan Gao,[a] Hiroki Ubukata,[a] Wenli Pan,[d] Kentaro Yamamoto,[d,e] Yoshihisa Uchimoto,[d] Akihide Kuwabara,[b*] Hiroshi Kageyama[a*]

[a] *Department of Energy and Hydrocarbon Chemistry, Graduate School of Engineering, Kyoto University, Nishikyo-ku, Kyoto 615-8510, Japan.*
[b] *Nanostructures Research Laboratory, Japan Fine Ceramics Center, Nagoya 456-8587, Japan.*
[c] *Division of Materials and Manufacturing Science, Graduate School of Engineering, Osaka University, Osaka 565-0871, Japan.*
[d] *Graduate School of Human and Environment Studies, Kyoto University, Sakyo-ku, Kyoto 606-8501, Japan*
[e] *Faculty of Engineering, Nara Women's University, Kitauoyanishimachi, Nara 630-8506, Japan.*

[*]Corresponding author: kuwabara@jfcc.or.jp and kage@scl.kyoto-u.ac.jp

Table of Contents:
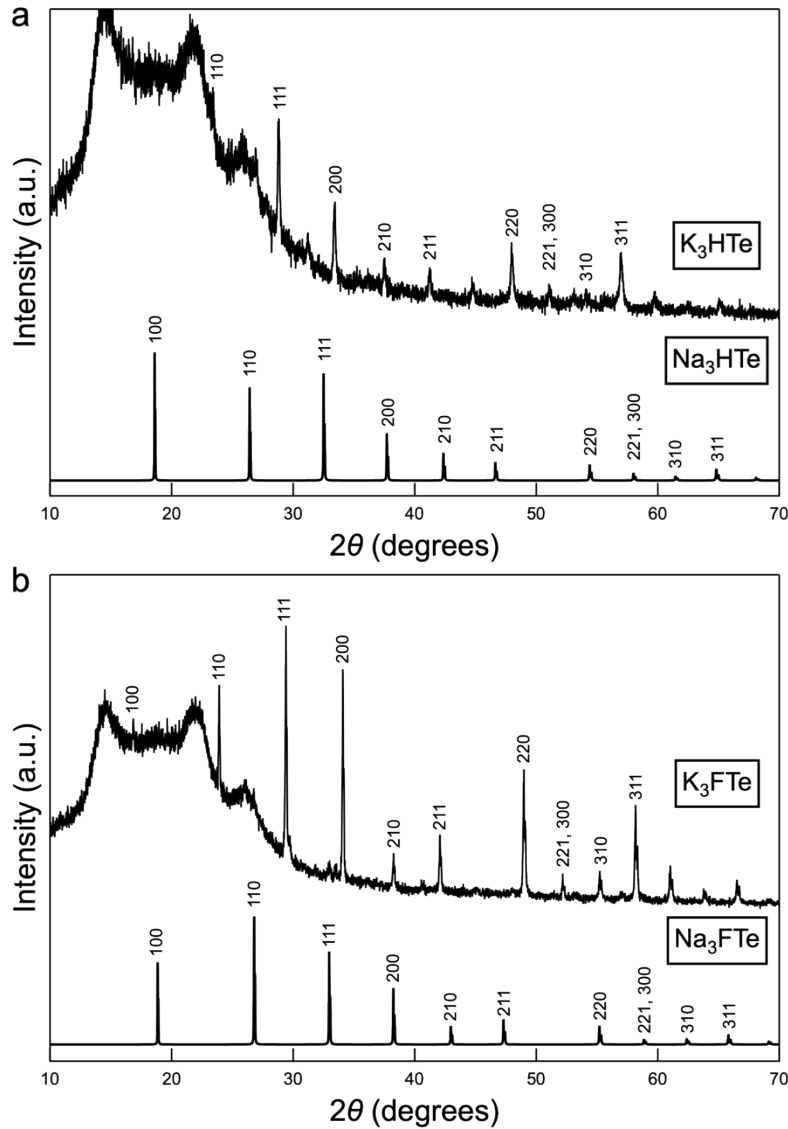
Section 1. XRD patterns of K₃HTe and K₃FTe

Figure S1 XRD patterns of (a) K₃HTe synthesized under high pressure using a mixture of KH and K₂Te in a molecular ratio of 2:1 and reported cubic Na₃HTe,[1] and (b) K₃FTe synthesized under high pressure using a mixture of KF and K₂Te in a molecular ratio of 1:1 and reported cubic Na₃FTe.[2] The diffraction peaks are indexed in a cubic symmetry and labelled with the Miller indices of the lattice planes.
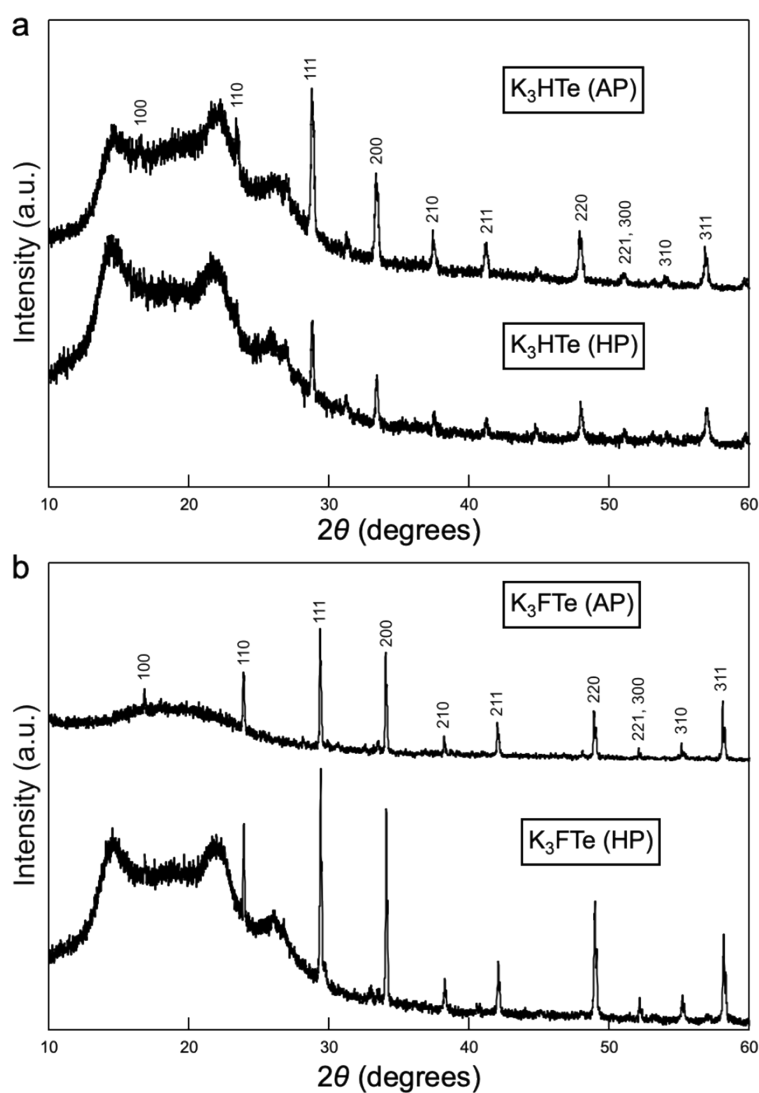
Figure S2 XRD patterns of (a) K$_3$FTe synthesized under ambient pressure (top) and under high pressure (bottom), and (b) K$_3$FTe synthesized under ambient pressure (top) and under high pressure (bottom). The diffraction peaks are indexed in a cubic symmetry and labelled with the Miller indices of the lattice planes. Almost the same diffraction patterns (i.e., almost the same lattice constants) are obtained for both conditions in both compounds.
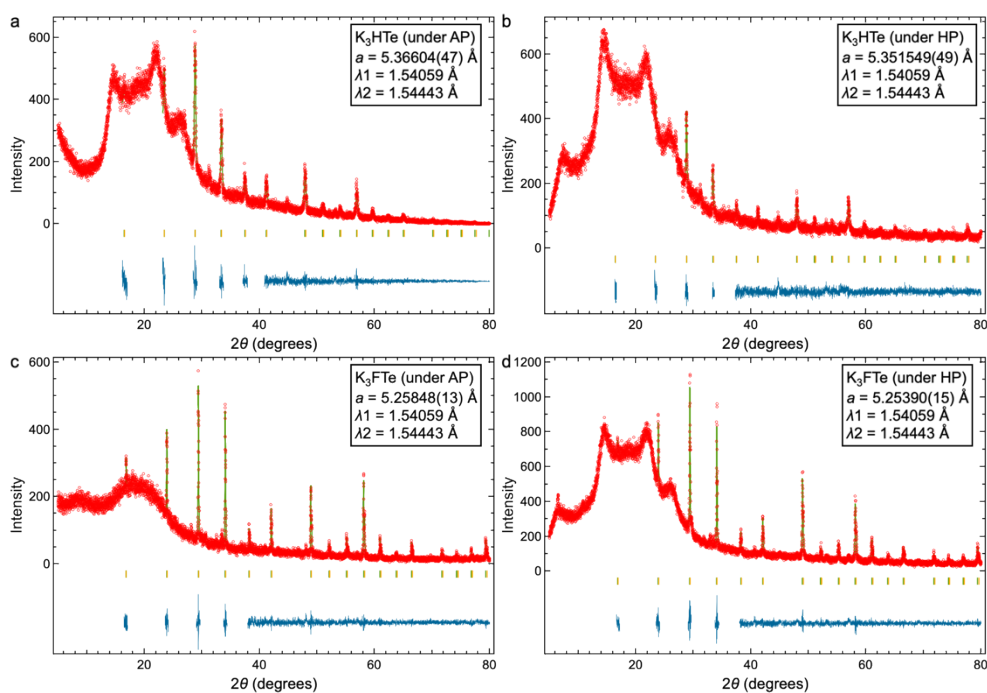
Figure. S3 Le Bail refinement for K$_3$HTe (a) synthesized under ambient pressure and (b) synthesized under high pressure and for K$_3$FTe (c) synthesized under ambient pressure and (d) synthesized under high pressure, respectively. The red circles, green solid lines, and blue solid lines represent the observed, calculated, and difference intensities, respectively. The green and yellow ticks indicate the calculated Bragg reflections from K$_{\alpha 1}$ and K$_{\alpha 2}$ Cu x-ray, respectively. The peak of Kapton tape in the low angle is removed from the refinement.

Section 2. Size-flexibility of soft anions

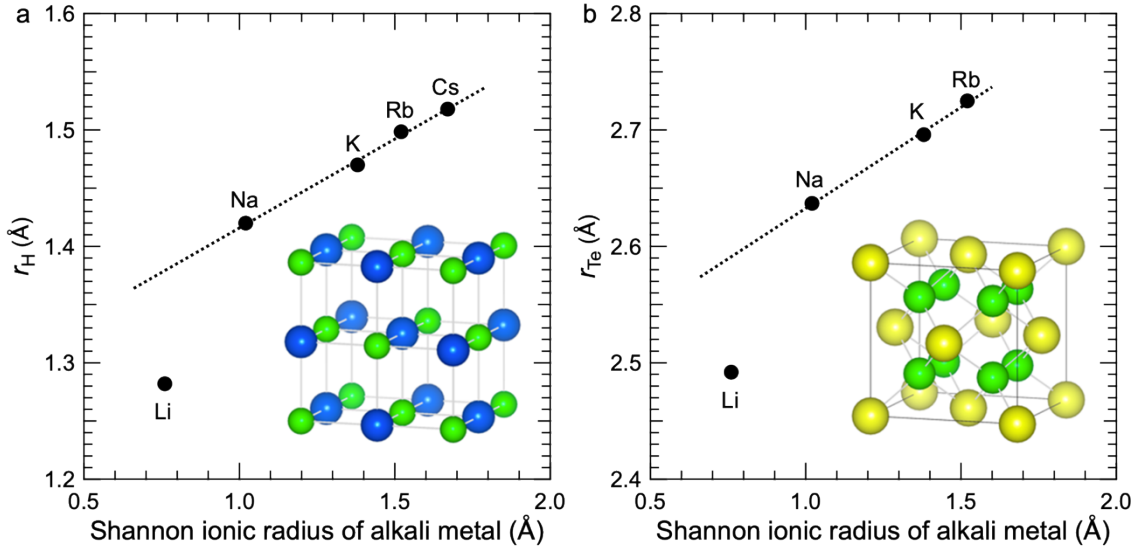**Figure S4** Size flexibility of (a) H in rock-salt type MH (M = Li, Na, K, Rb, Cs)[3,4] and (b) Te in anti-fluorite type M_2Te (M = Li, Na, K, Rb)[5,6] depending on the Shannon ionic radius[7] of alkali metal cation species (alkali metal: green, H: blue, Te: yellow). Unexpected contracts in the soft anions, H and Te, is seen in Li systems in each series. This is attributed to the surface charge density of the alkali metal as seen in antiperovskites M_3HTe and M_3FTe (M = Li, Na, K).

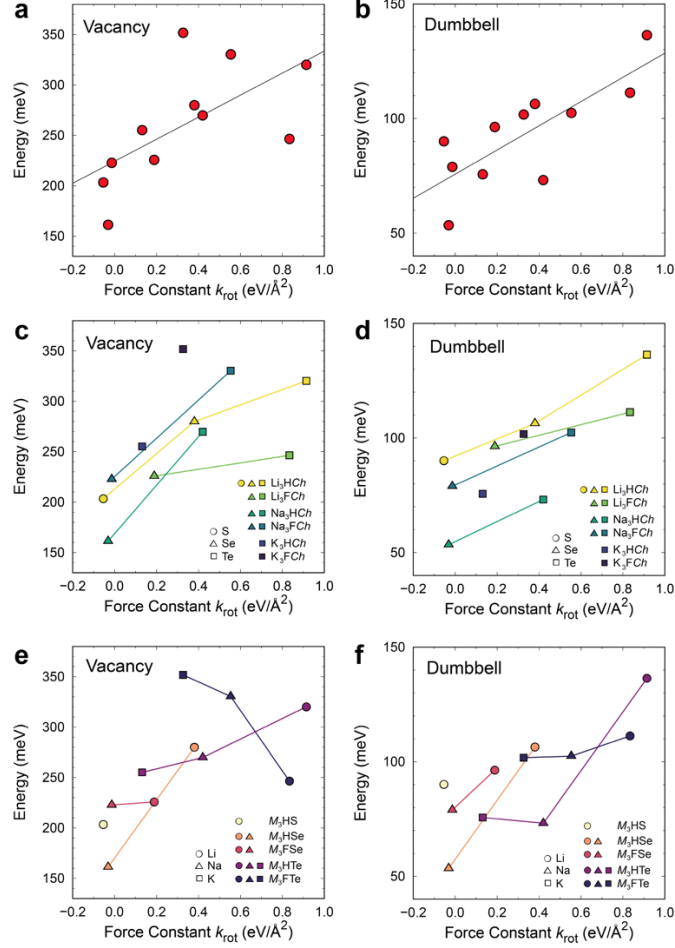Section 3. The migration barriers in K$_3$HTe and K$_3$FTe

Figure S5 (a,b) Migration energy barriers of M_3BCh (M = Li, Na, K; B = H,F; Ch = S, Se, Te) for (a) vacancy and (b) interstitial dumbbell mechanisms as a function of force constant k_{rot}. The migration energy barriers of Li- and Na-rich antiperovskites are taken from our previous papers.[1,2] k_{rot} is related to the rotational phonon mode of BM_6 and was estimated by the equation of simple harmonic motion $\omega_{rot} = \sqrt{k_{rot}/m_M}$, where ω_{rot} is the phonon frequency of the rotational mode at the M point and m_M is the atomic mass of M. Small k_{rot} indicates that the octahedron is more easily rotated (see our previous papers[1,2] for more details). The black line is a least-squares approximation of the points. The activation energy decreases with decreasing k_{rot} for both mechanisms, suggesting that k_{rot} is an important factor in determining the activation energy in M_3BCh. (c,d) Same as (a,b) but compounds are categorized into six groups: Li$_3$HCh, Li$_3$FCh, Na$_3$HCh, Na$_3$FCh, K$_3$HCh and K$_3$FCh. (e,f) Same as (a,b) but compounds are categorized into five groups:

M_3HS, M_3HSe, M_3FSe, M_3HTe, and M_3FTe. In (c) and (d), the activation energy decreases with increasing k_{rot} for each group, but the gradient and magnitude of energy are different. In (e) and (f), the activation energy decreases as k_{rot} decreases in most groups, though increases in M_3FTe with the vacancy mechanism. These results indicate that there are other factors influencing the activation energy than k_{rot}, such as the structural distortion in the vicinity of migrating M^+ ion.

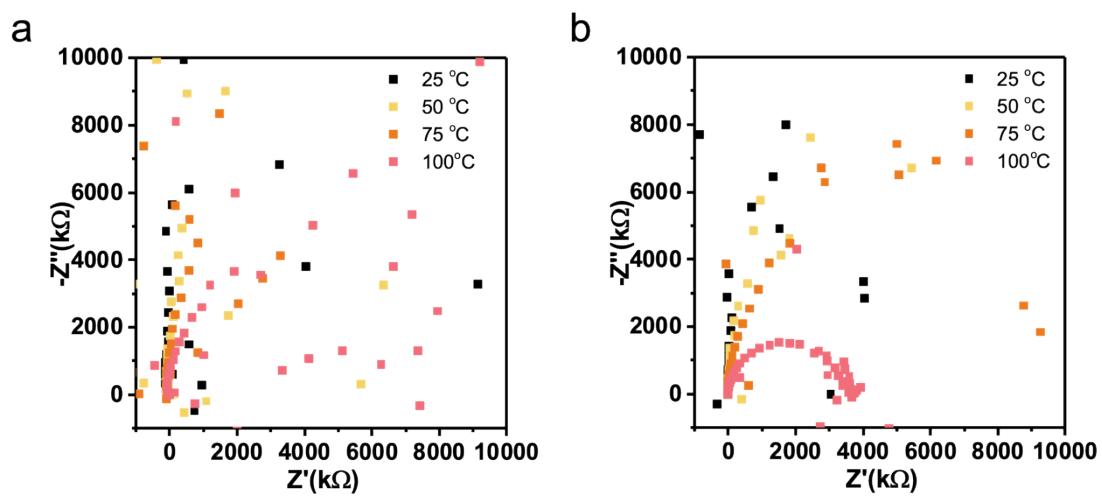Section 4. The ionic conduction of pristine and iodine substituted K_3HTe

Figure S6 Cole-Cole plots for (a) pristine K_3HTe and (b) iodine doped K_3HTe.

Section 5. Supplementary references

1   S. Gao, T. Broux, S. Fujii, C. Tassel, K. Yamamoto, Y. Xiao, I. Oikawa, H. Takamura,
     H. Ubukata, Y. Watanabe, K. Fujii, M. Yashima, A. Kuwabara, Y. Uchimoto and H.
     Kageyama, *Nat. Commun.*, 2021, **12**, 201.

2   S. Fujii, S. Gao, C. Tassel, T. Zhu, T. Broux, K. Okada, Y. Miyahara, A. Kuwabara
     and H. Kageyama, *J. Am. Chem. Soc.*, 2021, **143**, 10668–10675.

3   E. Zintl and A. Harder, *Z. Phys. Chem.*, 1931, **B14**, 265–284.

4   L. Elansari, L. Antoine, R. Janot, J. C. Gachon, J. J. Kuntz and D. Guérard, *J. Alloys
     Compd.*, 2001, **329**, 5–8.

5   E. Zintl, A. Harder and B. Dauth, *Ztschr. Elektrochem.*, 1934, **40**, 588–593.

6   H. Sommer and R. Hoppe, 1977, **429**, 118–130.

7   R. D. Shannon, *Acta Crystallogr. Sect. A*, 1976, **32**, 751–767.